nature climate change

Article

https://doi.org/10.1038/s41558-023-01897-w

Hydrological cycle amplification reshapes warming-driven oxygen loss in the Atlantic Ocean

Received: 25 December 2022

Accepted: 20 November 2023

Published online: 8 January 2024

Check for updates

Allison Hogikyan [1] ✉, Laure Resplandy [2,3], Maofeng Liu [4] & Gabriel Vecchi [2,3]

The loss of oxygen from the ocean due to warming is not ubiquitous. In the Atlantic Ocean above 1 km depth, there is oxygen loss at subpolar latitudes, but there has been no oxygen loss or gain in the subtropics over the past six decades. Here we show that the amplification of the hydrological cycle, a response to climate change that results in a 'salty-get-saltier, fresh-get-fresher' sea surface salinity pattern, influences ocean ventilation and introduces a spatial pattern in the rate of climate change-driven oxygen loss in an Earth system model. A salinification enhances ventilation of (already salty) mode waters that outcrop in the subtropics and opposes warming-driven oxygen loss, while a freshening reduces ventilation of (already fresh) deep waters that outcrop at subpolar latitudes and accelerates oxygen loss. These results suggest that climate change introduces patterns of oxygenation through surface salinity changes, key to understanding observed and future regional changes.

The oceans lose oxygen in response to global warming. This loss is attributed to the rise in ocean temperature, which decreases oxygen solubility and increases upper-ocean stratification. The increased stratification slows the supply of well-oxygenated waters from the surface to the ocean interior (by both mixing and transport), a process called ocean ventilation[1–10]. This ocean deoxygenation has the potential to enhance the production of nitrous oxide, a potent greenhouse gas[11–13], and compress the habitat of macro-organisms, with possible negative impacts for valuable fisheries[3,14,15]. Observations and modelling studies suggest that the globally integrated ocean oxygen content has declined by about 2% since the 1960s (for example, refs. 4,16) and that this loss could reach 6% in 2100 if emissions are not curtailed[1,17,18]. Oxygen changes are, however, highly variable in space, with regions losing oxygen at rates up to 40–50% while others are weakly gaining oxygen[19,20].

Regional patterns in oxygen changes are particularly strong in the Atlantic Ocean[19,21,22]. As shown in Fig. 1, observations over the past six decades suggest that subpolar and tropical regions have lost oxygen (rates down to −1 to −3 µmol kg^{-1} $decade^{-1}$), while subtropical regions have gained oxygen or experienced very weak changes (rates up to +1.5 µmol kg^{-1} $decade^{-1}$, mean trends over the surface to 1,000 m depth and 1950–2016). Ref. 21 showed that the rather unexpected oxygenation or near-zero change observed in the northern subtropical Atlantic Ocean was contained largely within salty water masses called mode waters that ventilate the subsurface ocean layers (typically 200–1,000 m). By contrast, they find a strong oxygen loss in fresh deep waters that form in the subpolar North Atlantic and then flow equatorward beneath mode waters. This contrast between oxygen changes in deep and mode waters is also present in the historical and future response of Earth system models to anthropogenic forcing (Fig. 2c). These models simulate weak oxygen changes or even an increase in salty North Atlantic Mode Waters, but particularly strong deoxygenation in fresher and deeper deep and bottom waters (see Fig. 1 in ref. 23 and Fig. 13 in ref. 1). The presence of this (de)oxygenation pattern in both

[1]Atmospheric and Oceanic Sciences Program, Princeton University, Princeton, NJ, USA. [2]Geosciences Department, Princeton University, Princeton, NJ, USA. [3]High Meadows Environmental Institute, Princeton University, Princeton, NJ, USA. [4]Rosenstiel School of Marine, Atmospheric, and Earth Science, University of Miami, Miami, FL, USA. ✉e-mail: hogikyan@princeton.edu

https://doi.org/10.1038/s41558-023-01897-w

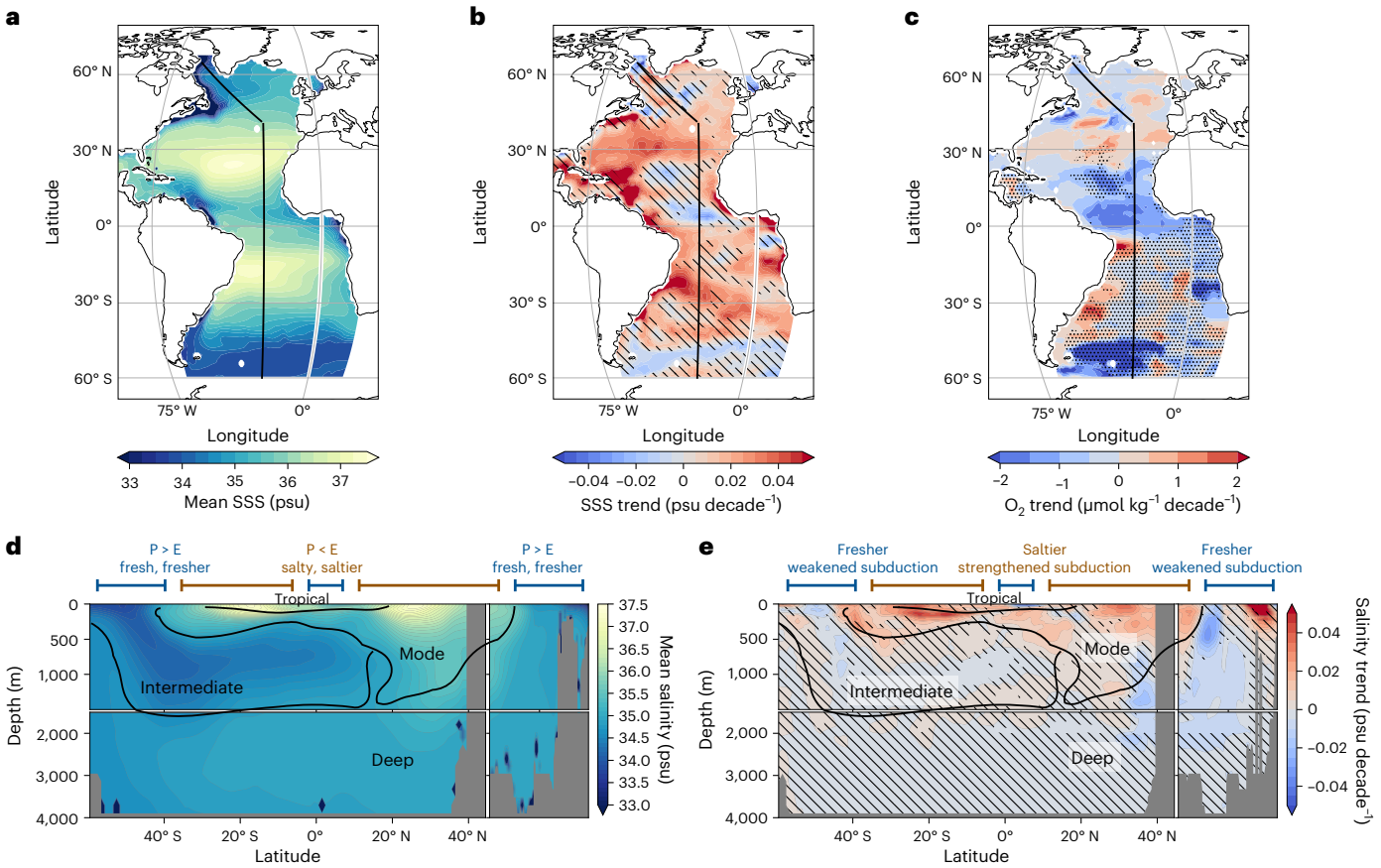


Fig. 1 | Historical observation-based changes in salinity and oxygen in the Atlantic Ocean. a,**b**, Mean (**a**) and linear trend (**b**) in SSS from five observation-based datasets (period 1968–2017): the European Centre for Medium-Range Weather Forecasts ORAS5 (ref. 58), the National Centers for Environmental Information's objective analysis[64], Japan Meteorological Agency's objective analysis[65], UK Hadley Centre's objective analysis EN4 (ref. 66) and the Institute of Atmospheric Physics' objective analysis CZ16 (ref. 67). Hatching indicates where not all datasets agree on the sign of the trend. **c**, Linear trend in average oxygen concentration in the upper 1,000 m of the ocean from the annual-mean[22] dataset (1950–2016 period). Stippling indicates where at least one depth level (out of 47) has fewer than 20 years of data from which to estimate the trend. **d**,**e**, Mean (**d**) and linear trend (**e**) in salinity in observation-based datasets along mid-Atlantic depth section (~25° W, shown in **a**–**c**, 1968–2017 period). Only ORAS5 and EN4 extend below 2 km depth. Hatching as in **b**. Water masses outlined in black (tropical, mode, intermediate and deep waters) are defined on the basis of density and salinity criteria (see Methods for details). Schematic in **d**,**e** points to the contrast between salty-get-saltier and fresh-get-fresher regions.

observations and the forced response of Earth system models suggests it is part of the response to climate change and not attributable to natural variability, but the mechanisms responsible are still unknown. In this Article, we show that the hydrological cycle amplification, a response to global warming that strengthens patterns of evaporation and precipitation[24] and sea surface salinity (SSS)[25,26], can alter the supply of oxygen to the ocean interior by ventilation and help explain the spatial pattern of oxygen changes in the Atlantic Ocean.

Mean global sea surface salinity (SSS) patterns have intensified (salty waters tend to become saltier while fresh waters become fresher) over the historical period, with the Atlantic becoming saltier and the Pacific becoming fresher[27–37]. Within the Atlantic Ocean, the contrast between the salty surface waters in the subtropics and relatively fresher waters in the tropical and subpolar regions has intensified (Fig. 1b), although the details of this pattern amplification are subject to uncertainty. Most notably, observation-based products disagree on whether the SSS has increased or decreased in the fresh Labrador Sea over the past five decades (for example, refs. 25,28,29,31,38 and hatching in Fig. 1b), despite the fact that longer-term observation-based reconstructions over the twentieth century (1890s to 2010s (refs. 32,33)) and Earth system models (for example, refs. 36,39) agree that this region has and will freshen in response to global warming, following the expected fresh-get-fresher pattern.

This 'salty-get-saltier, fresh-get-fresher' pattern is attributed largely to an amplification of the hydrological cycle in the atmosphere, a robust response of climate models to global warming (specifically, amplified moisture convergence in the atmosphere requires an amplification of surface moisture flux[24]). This mechanism largely explains the SSS changes observed in the Atlantic Ocean as it causes salty regions, where climatological evaporation exceeds climatological precipitation, to become saltier and fresh regions, where precipitation exceeds evaporation, to become fresher (for example, ref. 40) (Fig. 1a,b,e). This SSS pattern amplification is reinforced by increased upper-ocean stratification due to global warming, which limits the exchanges between ocean surface and interior, increasing the influence of mean air–sea freshwater fluxes on surface waters[26].

Changes in SSS influence surface water density and therefore the formation rate and transport (mixing, subduction and advection) of the water masses that ventilate and supply oxygen to the ocean interior. As evidenced by five observation-based data products, surface salinity changes in the Atlantic Ocean propagate into the ocean interior along the pathways of the main water masses (Fig. 1e). The salty tropical and mode waters, which supply oxygen to the surface and subsurface subtropical Atlantic Ocean down to 1,000 m depth, have become saltier (water masses labelled in Fig. 1d,e). By contrast, the fresher intermediate and deep waters, which are formed at subpolar

https://doi.org/10.1038/s41558-023-01897-w

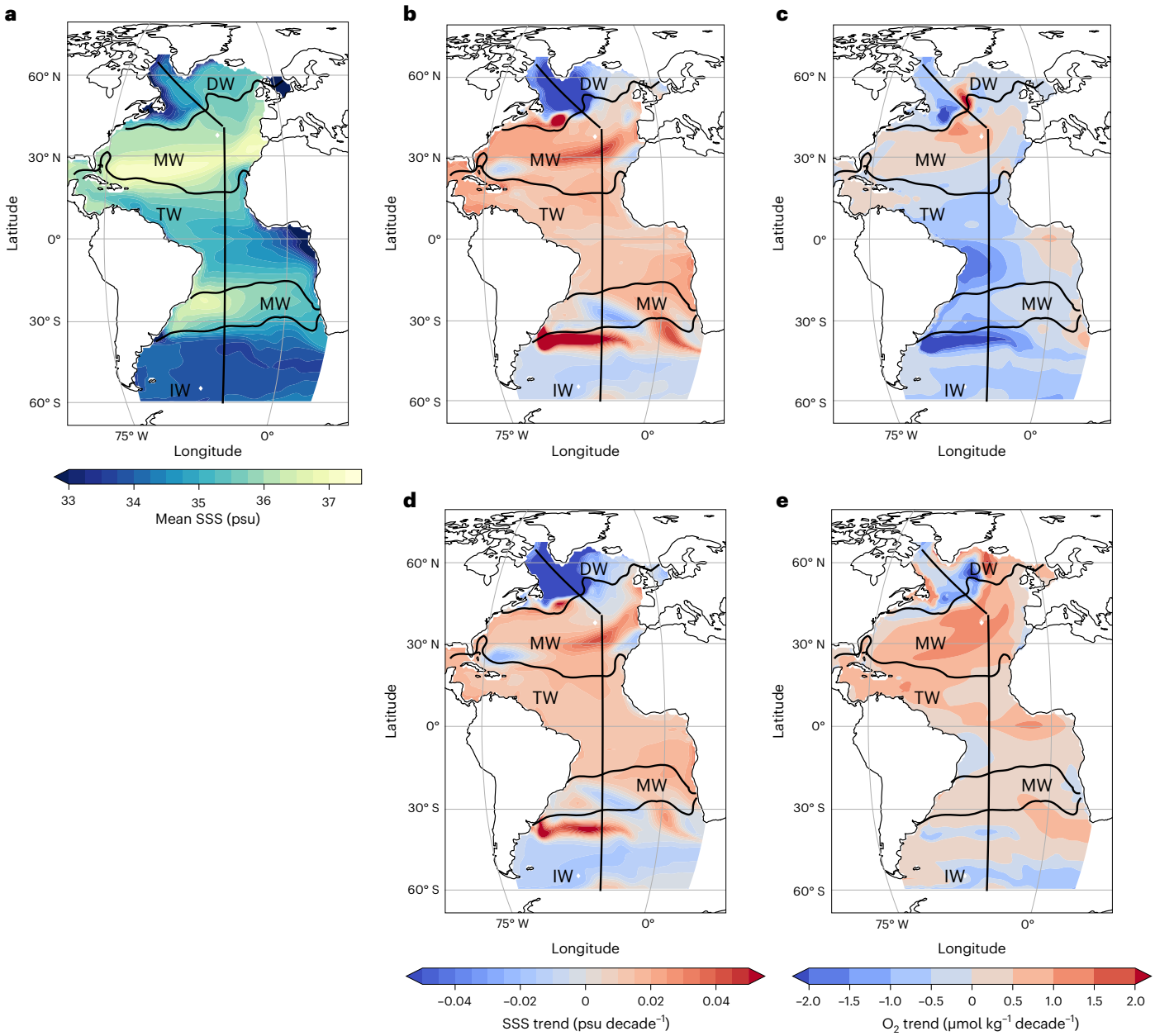


Fig. 2 | Salinity and oxygen changes simulated in response to total climate effect and hydrological effect. a, Mean SSS in pre-industrial control simulation. **b**,**c**, Climate effect in SSS (**b**) and upper 1,000 m oxygen concentration (**c**) (200 yr trends in 1%-to-doubling Standard experiment). **d**,**e**, Hydrological effect in SSS (**d**) and upper 1,000 m oxygen concentration (**e**) (200 yr trend difference between Standard and Fix-SSS experiments). Black contours denote surface outcrop of water masses. Straight black line is the path of the depth section followed in Figs. 3 and 5. DW, deep waters; MW, mode waters; TW, tropical waters; IW, intermediate waters.

latitudes and supply oxygen to the deep ocean underneath tropical and mode waters, have become fresher or experienced marginal changes in salinity (Fig. 1d,e). The strong increase in salinity where mode waters form was shown to efficiently de-stratify the surface layer despite the warming-driven stratification in a global climate model[41], which could potentially lead to deeper mixed layers and enhanced formation and ventilation of mode waters. The surface freshening at subpolar latitudes can, by the same logic, be expected to enhance warming-driven stratification and weaken the ventilation of deeper intermediate and deep waters[42–46]. The amplification of the hydrological cycle could therefore alleviate the warming-driven deoxygenation in salty water masses but reinforce it in fresher water masses, potentially explaining the observed pattern of subtropical oxygenation and subpolar deoxygenation (Fig. 1c).

Here we use a global Earth system model (ESM2M) to quantify the effect of amplified SSS patterns on Atlantic Ocean deoxygenation in an idealized global warming scenario. We compare a 'Standard' warming experiment in which the model evolves freely and SSS patterns amplify in response to atmospheric CO_2 increase (1% yr^{-1} CO_2 increase until doubling, then held constant during a total of 200 simulation years) with a 'Fix-SSS' experiment in which the same CO_2 increase is prescribed but SSS patterns do not respond and are instead restored towards their pre-industrial climatological values (similarly to ref. 41; see details in Methods). While warming occurs in both experiments (Extended Data Fig. 1), the ocean experiences hydrological cycle amplification only in the Standard experiment (and not in Fix-SSS). In this comparison, we emphasize the contrast between the salty mode waters and fresh deep waters, which respond strongly to the surface salinity changes

https://doi.org/10.1038/s41558-023-01897-w

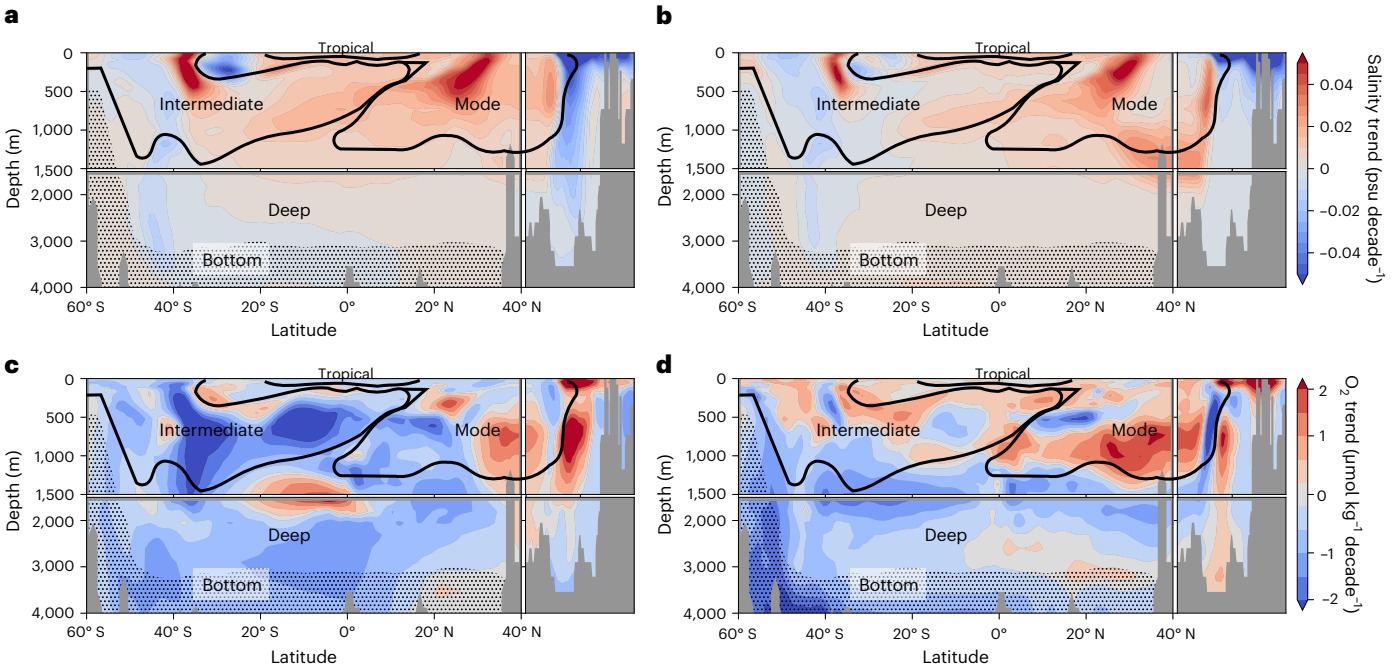


Fig. 3 | Salinity and oxygen changes in response to total climate effect and hydrological effect along mid-Atlantic Ocean section. a,**b**, Trends in salinity due to the climate effect (ΔS_{Clim}, 200 yr trend in Standard warming experiment) (**a**) and the hydrological effect (ΔS_{Hydro}; 200 yr trend in Standard warming experiment minus 200 yr trend in Fix-SSS experiment, each averaged over five ensemble members) (**b**). **c**,**d**, Trends in oxygen concentration from the climate effect ($\Delta O_{2,Clim}$) (**c**) and hydrological effect ($\Delta O_{2,Hydro}$) (**d**). Water masses along the mid-Atlantic section are outlined by black contours (see Methods and Fig. 1 for section location). Stippling indicates bottom waters, which are excluded from our analysis.

in their outcrop regions, and establish a mechanistic link among hydrological cycle amplification, salinity changes and patterns of ocean deoxygenation.

Amplification of salinity patterns in response to warming

The Earth system model ESM2M projects an amplification of salinity patterns in response to global warming (Fig. 2), consistent with the robust response identified previously in climate models[24,47,48]. We briefly compare the amplification of the salinity patterns in response to climate change, or total 'climate effect', in the ESM2M model (200 yr trend averaged across five ensemble members of the Standard 1%-to-doubling CO_2 increase experiment) and in a set of five observation-based datasets (1950s–2010s trends), emphasizing the range across the datasets. The surface salinification of the subtropics is weaker in the model than in the datasets, in particular along the western continental margins (+0.04 versus +0.06 psu decade^{-1}; Figs. 1b and 2b). The projected surface freshening of the Labrador Sea (−0.10 psu decade^{-1}) is consistent with the Ocean Re-Analysis 5 (ORAS5) reanalysis (Extended Data Fig. 2) and previous observation-based studies[27–33] but is inconsistent with the ensemble of reanalyses (Fig. 1b) and other observation-based studies[25,26,34,38,48]. These discrepancies across observational studies highlight the challenge of estimating salinity changes in this region but do not rule out a freshening in the Labrador Sea as the fingerprint of CO_2-forced warming on centennial timescales. In the following, we present the freshening in the Labrador Sea as the ESM2M response to CO_2 forced warming but note that it is uncertain whether the Labrador Sea will become increasingly fresh or salty in the coming decades.

The propagation of the surface salty-get-saltier and fresh-get-fresher signals into the ocean interior are remarkably similar in ESM2M and the observation-based datasets, despite some discrepancies at the surface (observations in Fig. 1e and Extended Data Fig. 3; model result in Fig. 3a). This includes the increase in salinity (up to +0.06 psu decade^{-1}) in mode and tropical waters formed in salty regions where evaporation increases and the freshening (up to −0.1 psu decade^{-1}) of deep waters that outcrop at higher northern latitudes where evaporation decreases (Figs. 1e and 3a; see precipitation and evaporation changes in Extended Data Fig. 5). Differences exist, however, between the model and datasets. Notably, as the South Atlantic subtropical gyre expands and the boundary between mode and intermediate waters moves polewards (a feature supported by satellite and in-situ observations[49,50]), it redistributes the volume of salty South Atlantic Mode Waters meridionally in the model (dipole of salinity change at ~35° S; Fig. 3a) but has a much weaker effect on salinity in observation-based datasets (Fig. 1e). Despite these differences, we use the model, which captures the amplification of salinity patterns and their propagation into the ocean interior, to demonstrate that these substantial changes in salinity influence the Atlantic Ocean ventilation and probably control the (de)oxygenation pattern observed in nature.

Stronger deoxygenation in fresher water masses

Fresher water masses (intermediate and deep waters) experience stronger deoxygenation and weaker salinity increase than saltier water masses (tropical and mode waters) in response to climate change in the ESM2M model (climate effect ΔS_{Clim} and $\Delta O_{2,Clim}$; Figs. 2b,c, 3 and 4a). When averaged over the full Atlantic basin, salty mode waters become saltier and avoid deoxygenation (ΔS_{Clim} = +0.020 (0.015 to 0.022) psu decade^{-1}, $\Delta O_{2,Clim}$ = −0.03 (−0.08 to +0.05) μmol kg^{-1} decade^{-1}; mean and range of five ensemble members; Fig. 4a and Methods). Tropical waters also become saltier but at a lower rate than mode waters (ΔS_{Clim} = +0.015 (0.013 to 0.017) psu decade^{-1}) and slightly lose oxygen ($\Delta O_{2,Clim}$ = −0.28)−0.29 to −0.27) μmol kg^{-1} decade^{-1}). By contrast, fresh intermediate and deep waters are characterized by the weakest salinity changes (ΔS_{Clim} < 0.007 psu decade^{-1}; Fig. 4a) and the strongest deoxygenation rates ($\Delta O_{2,Clim}$ = −0.83 (−0.87 to −0.80) and −0.60 (−0.64 to −0.53) μmol kg^{-1} decade^{-1}; Fig. 4a).

The absence of a strong freshening in intermediate and deep waters in the model may appear inconsistent with the fresh-get-fresher

https://doi.org/10.1038/s41558-023-01897-w

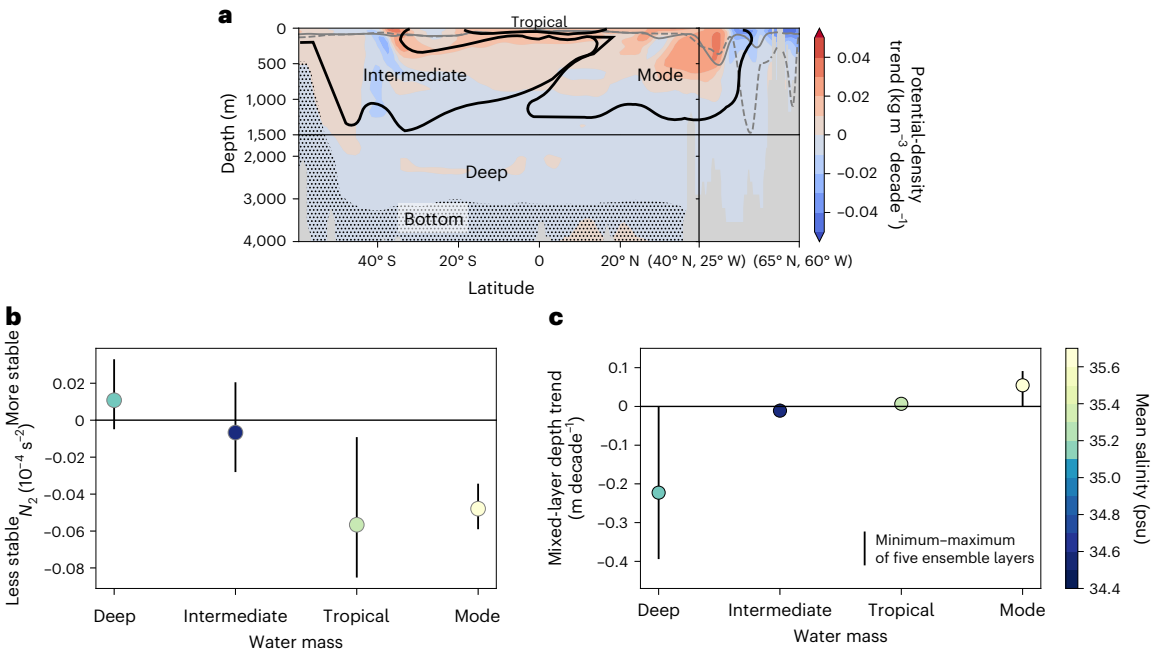


Fig. 4 | Hydrological effect on potential density, stability and mixed-layer depth. **a**, Hydrological effect in potential density (200 yr trend in Standard − Fix-SSS), following the trajectory along 25° W shown in Fig. 1 with black water-mass contours and grey annual-maximum mixed-layer depth contours (solid lines are mean over the past 50 years of Standard experiment while dashed lines are mean over the past 50 years of Fix-SSS experiment). Extended Data Fig. 4 estimates the contributions of salinity and temperature to this density trend difference. **b**, Hydrological effect (Standard − Fix-SSS) in squared Brunt–Väisälä frequency (N^2, a measure of vertical stability) at the base of the annual-maximum mixed layer. Dots indicate average difference (Standard − Fix-SSS) over the past 50 years of the experiments and over each water mass (as labelled on the *x* axis). **c**, Hydrological effect (200 yr trend in Standard − Fix-SSS) of annual-maximum mixed-layer depth. Black bars in **b**,**c** indicate the minimum–maximum range across the five ensemble members. Colours of dots in **b**,**c** indicate mean salinity of each water mass, following the colour bar to the right of **c**.

rule of thumb but is in fact consistent with the global ocean salinity pattern amplification. The Atlantic Ocean as a whole becomes saltier in contrast to the Pacific Ocean becoming fresher, pushing surface salinity trends towards higher values across the Atlantic (versus towards lower values in the Pacific). In addition, the freshening of intermediate waters associated with the precipitation increase at their outcrop surface is offset by notable cross-isopycnal mixing with salty mode waters in the ocean interior—a process known to contribute strongly to the mean state and changes in this water mass[51,52]—as well as the southward advection of mode waters into intermediate waters as the subtropical gyre expands polewards (Figs. 2b and 3a). These fresh Atlantic Ocean water masses would perhaps be better described by fresh-stay-fresher rather than fresh-get-fresher since they remain fresher than the other water masses in the basin but do not in fact change salinity strongly.

We isolate the salinity and oxygen changes associated with the hydrological cycle amplification, or 'hydrological effect', from the total climate effect using the difference between the Standard warming experiment and the Fix-SSS experiment, in which SSS is restored towards its pre-industrial values (Methods). The salinity trends attributed to the hydrological effect (ΔS_{Hydro} in Figs. 2d and 3b) closely match the salinity trends simulated in response to the full climate effect (ΔS_{Clim} in Figs. 2b and 3a). This is consistent with the understanding that salinity trends under climate change are attributable largely to hydrological cycle amplification[25]. Across the four water masses considered here, a stronger salinity increase is linked to a weaker oxygen decrease (Figs. 2e and 4b). The hydrological effect yields a strong oxygen gain in mode waters that experience rapid salinification ($\Delta O_{2,Hydro}$ = +0.44 (+0.40 to +0.46) µmol kg^{-1} decade^{-1}), a near-zero change in intermediate and tropical waters that experience milder salinification ($\Delta O_{2,Hydro}$ < +0.10 µmol kg^{-1} decade^{-1}) and a strong oxygen loss in deep waters that experience a near-zero salinification ($\Delta O_{2,Hydro}$ = −0.43 (−0.45 to −0.39) µmol kg^{-1} decade^{-1}) (Fig. 4b). The hydrological cycle amplification therefore contributes to the net pattern of deoxygenation due to climate change by modulating the amplitude of the oxygen loss due to the direct effect of warming (stratification increase and solubility decrease). Its impact is strongest in salty mode waters, where the oxygen gain due to the hydrological effect counteracts the warming-driven deoxygenation (yielding a marginal net change in response to the total climate effect), as well as in fresh deep waters, where it accounts for more than half of the net simulated deoxygenation (Figs. 2c,e and 4a,b).

Ventilation controls the deoxygenation pattern

We can attribute the simulated changes in oxygen in response to the hydrological effect to three factors: changes in ventilation, including the effects of mixing, subduction and transport ($\Delta O_{2,Hydro,vent}$), changes in solubility tied to warming or cooling of the water masses ($\Delta O_{2,Hydro,sat}$) and changes in biological activity, which we find have a negligible effect here except in tropical waters ($\Delta O_{2,Hydro,bio}$; see bars in Fig. 4c). Changes in ventilation control the pattern of oxygen gain in salty mode waters and oxygen loss in fresh deep waters, while changes in solubility associated with the redistribution of ocean heat content (see temperature changes in Extended Data Fig. 1) play a secondary role and modulate the magnitude of the net oxygen changes attributed to the hydrological effect (Fig. 4c). In mode waters, the substantial oxygen gain by ventilation ($\Delta O_{2,Hydro,vent}$ = +0.68 (+0.65 to +0.71) µmol kg^{-1}) is offset by about a third by solubility changes ($\Delta O_{2,Hydro,sat}$ = −0.23 (−0.25 to −0.20) µmol kg^{-1} decade^{-1}). In deep waters, the oxygen loss attributed to ventilation ($\Delta O_{2,Hydro,vent}$ = −0.30 (−0.33 to −0.27) µmol kg^{-1} decade^{-1}) is, by contrast, reinforced by the reduced solubility ($\Delta O_{2,Hydro,sat}$ = −0.12 (−0.13 to −0.12) µmol g^{-1} decade^{-1}; Fig. 4c).

The hydrological effect has little or no influence on the oxygenation of intermediate and tropical waters due to the near-complete compensation between the different contributions (ventilation, solubility

https://doi.org/10.1038/s41558-023-01897-w

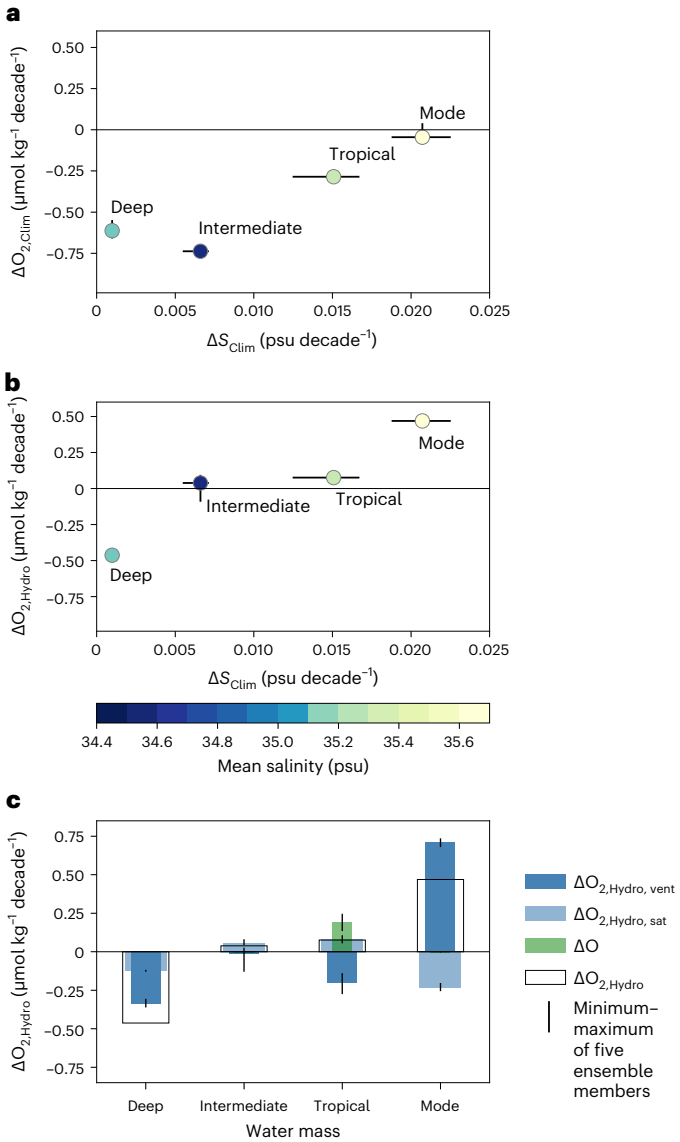


Fig. 5 | Oxygen and salinity changes across water masses and controlling mechanisms. a,**b**, Oxygen trends due to climate effect ($\Delta O_{2,Clim}$) (**a**) and hydrological effect ($\Delta O_{2,Hydro}$) (**b**) versus salinity trends in climate effect (ΔS_{Clim}, nearly identical to ΔS_{hydro}; Fig. 3). Filled circles represent the 200 yr trends averaged within each water mass across the five ensemble members, coloured using the mean salinity in the pre-industrial control experiment. Black error bars show the minimum–maximum range across the five ensemble members. (**c**) Attribution of hydrological effect ($\Delta O_{2,Hydro}$ in black empty bars, same values as **b**) to changes in ventilation ($\Delta O_{2,Hydro,vent}$, dark blue), solubility ($\Delta O_{2,Hydro,sat}$, light blue) and biological activity ($\Delta O_{2,Hydro,bio}$, green). $\Delta O_{2,Hydro,bio}$ is visible only in tropical waters because it is two to four orders of magnitude smaller than the other terms in other water masses. Error bars again show the range across the five ensemble members. Extended Data Fig. 6 shows the attribution of climate effect ($\Delta O_{2,Clim}$) to the same processes ($\Delta O_{2,Clim,sat}$, $\Delta O_{2,Clim,vent}$ and $\Delta O_{2,Clim,bio}$).

and biology; Fig. 4c). In intermediate waters, a small and uncertain decrease in oxygen supply by ventilation ($\Delta O_{2,Hydro,vent}$ = −0.07 (−0.18 to −0.03) kg^{-1} decade^{-1}) is entirely opposed by an equally small increase in oxygen solubility ($\Delta O_{2,Hydro,sat}$ = +0.08 (0.06 to 0.11) µmol kg^{-1} decade^{-1}). In tropical waters, the hydrological effect leads to a reduction in oxygen due to ventilation ($\Delta O_{2,Hydro,vent}$ = −0.20 (−0.28 to −0.14) µmol kg^{-1} decade^{-1}), offset by an increase in the biological production of oxygen ($\Delta O_{2,Hydro,bio}$ = +0.19 (+0.13 to +0.25) µmol kg^{-1} decade^{-1} controlled by increased photosynthesis; Extended Data Fig. 7) and an increase in oxygen solubility ($\Delta O_{2,Hydro,sat}$ = +0.08 (+0.05 to +0.11) µmol kg^{-1} decade^{-1}). This response of tropical waters is, however, a surface signal (tropical waters are shallower than 100 m) with little effect on the ocean interior.

Oxygen patterns consistent with ocean circulation changes

The hydrological effect enhances the ventilation of mode waters and weakens the ventilation of deep waters by influencing the vertical density structure, the depth of winter mixed layers in outcrop regions and the strength of the shallow and deep overturning circulations carrying these water masses into the ocean interior. The amplification of surface salinity patterns increases upper-ocean density (0 to 1,000 m depth) in subtropical salty-get-saltier regions but reduces it in fresh-get-fresher regions such as the Labrador Sea, where Deep Waters form (Fig. 5a and Extended Data Fig. 4). This patterned change in density influences the stability at the base of the winter (annual-maximum) mixed layer as in ref. 37 and the depth of the winter mixed layers, which are the primary control on the volumes of mode and deep waters that are entrained and formed each year. The hydrological effect destabilizes the upper ocean (−0.05 (−0.06 to −0.04) × 10^{-4} s^{-2}) and deepens winter mixed layers in regions where mode waters outcrop (+0.05 (0.03 to 0.09) m decade^{-1} on average in outcrop region), consistent with the increased oxygen supply by ventilation simulated in these waters (Fig. 5b). Locally, this salinity-driven deepening of winter mixed layers can be stronger. This is the case at the boundary between the subtropical and subpolar gyres, where winter mixed layers are 150 m deeper during the last 50 years of the Standard warming experiment than in the Fix-SSS experiment (compare solid and dashed grey lines at 40-45° N in Fig. 5a), implying an increased rate of mode waters formation. By contrast, the surface stabilizes (+0.01 (0 to 0.03) × 10^{-4} s^{-2}) and winter mixed layers shallow (−0.22 (−0.39 to −0.06) m decade^{-1}) where deep waters outcrop, leading to the reduced supply of oxygen by ventilation in these waters (Fig. 5b). For example, in the Labrador Sea, winter mixed layers extend down to 1,000 m in the Fix-SSS experiment (dashed grey line in Fig. 5a) but to only 500 m during the last 50 years of the Standard warming experiment (solid grey line in Fig. 5a), indicating that surface salinity strongly modulates the depth of winter mixing and deep waters formation rate.

The changes in density associated with the hydrological effect also influence the transport of these water masses in the ocean interior. The shallow overturning subtropical cells are stronger during the last 50 years of the Standard warming experiment (15.3 Sv) than in the Fix-SSS experiment (14.1 Sv, shallow overturning index calculated as the difference between the maximum of the Atlantic meridional overturning streamfunction between 12° N and 16° N and the minimum between 12° N and 16° S above 200 m depth; adapted from ref. 53). This result, along with the enhanced winter mixing in salty-get-saltier regions, indicates that both the formation and transport of mode waters into the ocean's interior are enhanced by the surface salinity increase. By contrast, the strength of the deep Atlantic meridional overturning circulation (AMOC) is slightly weaker in the last 50 years of the Standard experiment than in the Fix-SSS experiment (by 0.6 Sv, AMOC strength estimated as the maximum of the streamfunction between 10° N and 60° N over all depths; for example, ref. 54). This slowing of AMOC is consistent with idealized model 'hosing' experiments in which freshwater is added in large volumes to regions of deep water formation[46,47]. The difference in AMOC between the two experiments presented here is a small fraction of the total AMOC strength, but together with the changes in density and winter mixed layers, it suggests that hydrological cycle amplification slightly reduces the formation rate and transport of deep waters in the Atlantic Ocean on multidecadal timescales.

Changes in oxygenation tied to ventilation are milder in intermediate and tropical waters (Fig. 4c). The marginal change simulated in intermediate waters arises from the offsetting effects of surface

freshening at the outcrop surface, which tend to reduce upper-ocean density and oxygen supply by ventilation, and the salinification within the water mass caused by the poleward advection of, and mixing with, salty mode waters (as described in Stronger deoxygenation in fresher water masses), which tend to increase density and promote ventilation (Fig. 5). In tropical waters, the weak deoxygenation attributed to ventilation is consistent with the salinification and densification of the upper ocean, which slightly increase the mixing of low-oxygen subsurface waters into this small near-surface volume of relatively well-oxygenated waters.

Influence on ocean heat content and oxygen solubility

The changes in physical circulation associated with the hydrological amplification redistribute ocean heat content, explaining the changes in oxygen solubility (light blue bars in Fig. 4c). On average, mode and deep waters warm in response to the hydrological effect, whereas intermediate and tropical waters cool, although these temperature changes are not homogeneous in space across each water mass (Extended Data Fig. 1e–g). In mode waters, the mean warming can be attributed to the salinity-driven increase in ventilation (deeper mixed layers and stronger shallow overturning) that enhances their heat uptake[41]. In deep waters, the hydrological effect weakens the ventilation (shallower winter mixed layer and slightly weaker AMOC), which reduces the temperature of the Labrador Sea region (north of 45° N in Extended Data Fig. 1). Yet weakened mixing with very cold bottom waters in the Standard experiment (relative to the Fix-SSS) leads to a weak warming of most of the deep waters volume, which exceeds the more localized cooling in the formation regions and controls the reduction in oxygen solubility. In intermediate waters, the slight cooling and reduction in oxygen solubility are tied to the surface freshening, which causes a local decrease in ocean heat uptake (but is partly offset by the intruding and rapidly warming mode waters; Extended Data Fig. 1). Finally, tropical waters have a large surface area in contact with the atmosphere and are therefore influenced mostly by the surface cooling associated with the hydrological effect (more heat uptake in mode waters leads to surface cooling; see Extended Data Fig. 1 and refs. 41,55).

Limitations and caveats

The prominent role of ventilation in controlling the oxygen changes attributed to the hydrological effect (compared with biological and solubility changes) is consistent with previous findings showing that ocean circulation dominates decadal to multidecadal oxygen changes in both observation-constrained datasets and climate models (for example, refs. 7,10,56). Yet the exact magnitude of the ventilation changes that can be attributed to the hydrological cycle amplification is subject to uncertainty. We note, in particular, that the increase in salinity simulated in the subtropics in the model is lower than in the observation-based products. This underestimation of the hydrological cycle amplification and associated low-latitude salinification in the model is partly due to the slower warming simulated in the Standard experiment (global surface warming of 0.1 K decade^{-1} on average over the 200 years) relative to the historical period (global surface warming of 0.2 K decade^{-1} for 1960–2018 (ref. 57)). As a result, the increase in ventilation and oxygenation associated with the hydrological effect in mode waters might have been stronger over the past five decades than the simulated trend here. By contrast, the simulated subpolar freshening attributed to hydrological cycle amplification in the model might be overestimated because part of the signal might be associated with the transport of freshwater originating from sea-ice melt in the Arctic and not with changes in precipitation and evaporation (polewards of 80° N; see details on surface salinity restoring in Methods). Furthermore, the magnitude of the freshening in the Labrador Sea simulated in the Earth system model used here and in others[36] is uncertain. Indeed, observation-based reconstructions of SSS trends since 1950 support a freshening (−0.01 psu decade^{-1} (refs. 27–31)), in close agreement with longer reconstructions over the twentieth century (since 1896 (refs. 32,33)) and the ORAS5 reanalysis[58], whereas other reanalyses[26,34,48] and reconstructions[25,38] suggest that SSS has increased in and around the Labrador Sea since 1950 (at +0.02 to 0.1 psu decade^{-1}). The reduced ventilation and deoxygenation of deep waters simulated in this study might therefore not represent the changes of the historical period, but they can be interpreted as the response to a strong freshening.

Conclusions

The patterned change in oxygen identified here in response to the hydrological cycle amplification adds important nuance to the expectation that warming-driven decreases in both solubility and ventilation cause widespread deoxygenation (for example, refs. 1,2,4,59,60). Salty-get-saltier mode waters formed in the subtropics experience enhanced ventilation, opposing the effect of warming-driven oxygen loss. By contrast, fresh-get-fresher deep waters formed at subpolar latitudes experience reduced ventilation, adding to the oxygen loss expected from warming. Although tropical and intermediate waters respond more weakly to hydrological cycle amplification, the changes in these water masses support the link between increased salinity and increased ventilation. In the model, this hydrological effect strongly modulates the overall response to climate change (climate effect), possibly explaining the previously unaccounted-for oxygenation of Atlantic Mode Waters observed in nature[21].

The hydrological effect can be expected to modulate ocean ventilation outside the Atlantic Ocean. Yet projected salinity changes in the Pacific and Indian oceans are weaker than in the Atlantic[38], so that the contribution to oxygen changes is expected to be weaker in those basins. Finally, the link among salinity, ventilation and oxygen patterns identified here on multidecadal timescales may also operate on shorter interannual to decadal timescales, in response to natural oscillations that affect the distribution of rainfall and evaporation (for example, North Atlantic Oscillation[61,62]). On longer, multicentennial, timescales, however, changes in SSS may be more strongly influenced by ice-sheet melt than precipitation and evaporation. This could reinforce high-latitude freshening (for example, ref. 63) and weaken the ventilation and oxygenation of the deep water masses.

Online content

Any methods, additional references, Nature Portfolio reporting summaries, source data, extended data, supplementary information, acknowledgements, peer review information; details of author contributions and competing interests; and statements of data and code availability are available at https://doi.org/10.1038/s41558-023-01897-w.

References

1. Bopp, L. et al. Multiple stressors of ocean ecosystems in the 21st century: projections with CMIP5 models. *Biogeosciences* **10**, 6225–6245 (2013).
2. Stramma, L., Johnson, G. C., Sprintall, J. & Mohrholz, V. Expanding oxygen-minimum zones in the tropical oceans. *Science* **320**, 655–658 (2008).
3. Stramma, L. et al. Expansion of oxygen minimum zones may reduce available habitat for tropical pelagic fishes. *Nat. Clim. Change* **2**, 33–37 (2012).
4. Schmidtko, S., Stramma, L. & Visbeck, M. Decline in global oceanic oxygen content during the past five decades. *Nature* **542**, 335–339 (2017).
5. Prince, E. D. et al. Ocean scale hypoxia-based habitat compression of Atlantic istiophorid billfishes. *Fish. Oceanogr.* **19**, 448–462 (2010).
6. Palter, J. B. & Trossman, D. S. The sensitivity of future ocean oxygen to changes in ocean circulation. *Glob. Biogeochem. Cycles* **32**, 738–751 (2018).

7. Couespel, D., Lévy, M. & Bopp, L. Major contribution of reduced upper ocean oxygen mixing to global ocean deoxygenation in an Earth system model. *Geophys. Res. Lett.* **46**, 12239–12249 (2019).
8. Oschlies, A., Brandt, P., Stramma, L. & Schmidtko, S. Drivers and mechanisms of ocean deoxygenation. *Nat. Geosci.* **11**, 467–473 (2018).
9. Claret, M. et al. Rapid coastal deoxygenation due to ocean circulation shift in the northwest Atlantic. *Nat. Clim. Change* **8**, 868–872 (2018).
10. Portela, E., Kolodziejczyk, N., Vic, C. & Thierry, V. Physical mechanisms driving oxygen subduction in the global ocean. *Geophys. Res. Lett.* **47**, e2020GL089040 (2020).
11. Arevalo-Martínez, D. L., Kock, A., Löscher, C., Schmitz, R. A. & Bange, H. W. Massive nitrous oxide emissions from the tropical South Pacific Ocean. *Nat. Geosci.* **8**, 530–533 (2015).
12. Babbin, A. R., Bianchi, D., Jayakumar, A. & Ward, B. B. Rapid nitrous oxide cycling in the suboxic ocean. *Science* **348**, 1127–1129 (2015).
13. Ji, Q., Buitenhuis, E., Suntharalingam, P., Sarmiento, J. L. & Ward, B. B. Global nitrous oxide production determined by oxygen sensitivity of nitrification and denitrification. *Glob. Biogeochem. Cycles* **32**, 1790–1802 (2018).
14. Chu, J. W. & Tunnicliffe, V. Oxygen limitations on marine animal distributions and the collapse of epibenthic community structure during shoaling hypoxia. *Glob. Change Biol.* **21**, 2989–3004 (2015).
15. Vedor, M. et al. Climate-driven deoxygenation elevates fishing vulnerability for the ocean's widest ranging shark. *eLife* **10**, e62508 (2021).
16. IPCC *Special Report on the Ocean and Cryosphere in a Changing Climate* (eds Pörtner, H.-O. et al.) (Cambridge Univ. Press, 2019).
17. Kwiatkowski, L. et al. Twenty-first century ocean warming, acidification, deoxygenation, and upper-ocean nutrient and primary production decline from CMIP6 model projections. *Biogeosciences* **17**, 3439–3470 (2020).
18. Lévy, M., Resplandy, L., Palter, J. B., Couespel, D. & Lachkar, Z. Chapter 13: The crucial contribution of mixing to present and future ocean oxygen distribution in *Ocean Mixing: Drivers, Mechanisms and Impacts* (eds Meredith, M. & Garabato, A. N.) 329–344 (Elsevier, 2022).
19. Helm, K. P., Bindoff, N. L. & Church, J. A. Observed decreases in oxygen content of the global ocean. *Geophys. Res. Lett.* **38,** 23602 (2011).
20. Levin, L. A. Manifestation, drivers, and emergence of open ocean deoxygenation. *Ann. Rev. Mar. Sci.* **10**, 229–260 (2018).
21. Stendardo, I. & Gruber, N. Oxygen trends over five decades in the North Atlantic. *J. Geophys. Res. Oceans* **117,** 11004 (2012).
22. Ito, T., Minobe, S., Long, M. C. & Deutsch, C. Upper ocean O_2 trends: 1958–2015. *Geophys. Res. Lett.* **44**, 4214–4223 (2017).
23. Oschlies, A. et al. Patterns of deoxygenation: sensitivity to natural and anthropogenic drivers. *Phil. Trans. R. Soc. A* **375**, 20160325 (2017).
24. Held, I. M. & Soden, B. J. Robust responses of the hydrological cycle to global warming. *J. Clim.* **19**, 5686–5699 (2006).
25. Durack, P. J., Wijffels, S. E. & Matear, R. J. Ocean salinities reveal strong global water cycle intensification during 1950 to 2000. *Science* **336**, 455–458 (2012).
26. Zika, J. D. et al. Improved estimates of water cycle change from ocean salinity: the key role of ocean warming. *Environ. Res. Lett.* **13**, 074036 (2018).
27. Brewer, P. et al. A climatic freshening of the deep Atlantic north of 50°N over the past 20 years. *Science* **222**, 1237–1239 (1983).
28. Curry, R., Dickson, B. & Yashayaev, I. A change in the freshwater balance of the Atlantic Ocean over the past four decades. *Nature* **426**, 826–829 (2003).
29. Yashayaev, I. Hydrographic changes in the Labrador Sea, 1960–2005. *Prog. Oceanogr.* **73**, 242–276 (2007).
30. Read, J. F. & Gould, W. J. Cooling and freshening of the subpolar North Atlantic Ocean since the 1960s. *Nature* **360**, 55–57 (1992).
31. Dickson, B. et al. Rapid freshening of the deep North Atlantic Ocean over the past four decades. *Nature* **416**, 832–837 (2002).
32. Reverdin, G. et al. North Atlantic extratropical and subpolar gyre variability during the last 120 years: a gridded dataset of surface temperature, salinity, and density. part 1: dataset validation and rms variability. *Ocean Dyn.* **69**, 385–403 (2019).
33. Friedman, A. R., Reverdin, G., Khodri, M. & Gastineau, G. A new record of Atlantic sea surface salinity from 1896 to 2013 reveals the signatures of climate variability and long-term trends. *Geophys. Res. Lett.* **44**, 1866–1876 (2017).
34. Skliris, N. et al. Salinity changes in the world ocean since 1950 in relation to changing surface freshwater fluxes. *Clim. Dyn.* **43**, 709–736 (2014).
35. Skliris, N., Zika, J. D., Nurser, G., Josey, S. A. & Marsh, R. Global water cycle amplifying at less than the Clausius–Clapeyron rate. *Sci. Rep.* **6**, 38752 (2016).
36. Cheng, L. et al. Improved estimates of changes in upper ocean salinity and the hydrological cycle. *J. Clim.* **33**, 10357–10381 (2020).
37. Sallée, J.-B. et al. Summertime increases in upper-ocean stratification and mixed-layer depth. *Nature* **591**, 592–598 (2021).
38. Durack, P. J. & Wijffels, S. E. Fifty-year trends in global ocean salinities and their relationship to broad-scale warming. *J. Clim.* **23**, 4342–4362 (2010).
39. Sun, Q. & Du, Y. Sea surface salinity changes and trans-basin water vapor transport between the Atlantic and Pacific under CMIP6 abrupt-4xCO_2 scenario. *Clim. Dyn.* **60**, 1907–1924 (2023).
40. Bindoff, N. L. et al. in *Special Report on the Ocean and Cryosphere in a Changing Climate* (eds Pörtner, H.-O. et al.) 477–587 (Cambridge Univ. Press, 2019).
41. Liu, M., Vecchi, G., Soden, B., Yang, W. & Zhang, B. Enhanced hydrological cycle increases ocean heat uptake and moderates transient climate change. *Nat. Clim. Change* **11**, 848–853 (2021).
42. Drijfhout, S., Van Oldenborgh, G. J. & Cimatoribus, A. Is a decline of AMOC causing the warming hole above the North Atlantic in observed and modeled warming patterns? *J. Clim.* **25**, 8373–8379 (2012).
43. Cheng, W., Chiang, J. C. & Zhang, D. Atlantic meridional overturning circulation (AMOC) in CMIP5 models: RCP and historical simulations. *J. Clim.* **26**, 7187–7197 (2013).
44. Fan, Y., Lu, J. & Li, L. Mechanism of the centennial subpolar North Atlantic cooling trend in the FGOALS-g2 historical simulation. *J. Geophys. Res. Oceans* **126**, e2021JC017511 (2021).
45. Zhu, C. & Liu, Z. Weakening Atlantic overturning circulation causes South Atlantic salinity pile-up. *Nat. Clim. Change* **10**, 998–1003 (2020).
46. Stouffer, R. J. et al. Investigating the causes of the response of the thermohaline circulation to past and future climate changes. *J. Clim.* **19**, 1365–1387 (2006).
47. Manabe, S. & Stouffer, R. J. Simulation of abrupt climate change induced by freshwater input to the North Atlantic Ocean. *Nature* **378**, 165–167 (1995).
48. Skliris, N., Marsh, R., Mecking, J. V. & Zika, J. D. Changing water cycle and freshwater transports in the Atlantic Ocean in observations and CMIP5 models. *Clim. Dyn.* **54**, 4971–4989 (2020).
49. Drouin, K. L., Lozier, M. S. & Johns, W. E. Variability and trends of the South Atlantic subtropical gyre. *J. Geophys. Res. Oceans* **126**, e2020JC016405 (2021).
50. Yang, H. et al. Poleward shift of the major ocean gyres detected in a warming climate. *Geophys. Res. Lett.* **47**, e2019GL085868 (2020).

51. Talley, L. D. *Descriptive Physical Oceanography: An Introduction* (Academic Press, 2011).
52. Iudicone, D. et al. The formation of the ocean's anthropogenic carbon reservoir. *Sci. Rep.* **6**, 35473 (2016).
53. Lohmann, K. & Latif, M. Tropical Pacific decadal variability and the subtropical–tropical cells. *J. Clim.* **18**, 5163–5178 (2005).
54. Dunne, J. P. et al. GFDL's ESM2 global coupled climate–carbon Earth system models. Part I: physical formulation and baseline simulation characteristics. *J. Clim.* **25**, 6646–6665 (2012).
55. Williams, P. D., Guilyardi, E., Sutton, R., Gregory, J. & Madec, G. A new feedback on climate change from the hydrological cycle. *Geophys. Res. Lett.* **34**, 08706 (2007).
56. Feucher, C., Portela, E., Kolodziejczyk, N. & Thierry, V. Subpolar gyre decadal variability explains the recent oxygenation in the Irminger Sea. *Commun. Earth Environ.* **3**, 279 (2022).
57. Rohde, R. A. & Hausfather, Z. The Berkeley Earth land/ocean temperature record. *Earth Syst. Sci. Data* **12**, 3469–3479 (2020).
58. Zuo, H., Balmaseda, M. A., Tietsche, S., Mogensen, K. & Mayer, M. The ECMWF operational ensemble reanalysis–analysis system for ocean and sea ice: a description of the system and assessment. *Ocean Sci.* **15**, 779–808 (2019).
59. Keeling, R. F., Körtzinger, A. & Gruber, N. et al. Ocean deoxygenation in a warming world. *Annu. Rev. Mar. Sci* **2**, 199–229 (2010).
60. Bopp, L., Le Quéré, C., Heimann, M., Manning, A. C. & Monfray, P. Climate-induced oceanic oxygen fluxes: implications for the contemporary carbon budget. *Glob. Biogeochem. Cycles* https://doi.org/10.1029/2001GB001445 (2002).
61. Johnson, G. C. & Gruber, N. Decadal water mass variations along 20°W in the northeastern Atlantic Ocean. *Prog. Oceanogr.* **73**, 277–295 (2007).
62. Frölicher, T. L., Joos, F., Plattner, G., Steinacher, M. & Doney, S.C. Natural variability and anthropogenic trends in oceanic oxygen in a coupled carbon cycle–climate model ensemble. *Glob. Biogeochem. Cycles* **23**, GB1003 (2009).
63. Golledge, N. R. et al. Global environmental consequences of twenty-first-century ice-sheet melt. *Nature* **566**, 65–72 (2019).
64. Levitus, S. et al. World ocean heat content and thermosteric sea level change (0–2000 m), 1955–2010. *Geophys. Res. Lett.* **39**, 10603 (2012).
65. Ishii, M. et al. Accuracy of global upper ocean heat content estimation expected from present observational data sets. *Sola* **13**, 163–167 (2017).
66. Good, S. A., Martin, M. J. & Rayner, N. A. En4: quality controlled ocean temperature and salinity profiles and monthly objective analyses with uncertainty estimates. *J. Geophys. Res. Oceans* **118**, 6704–6716 (2013).
67. Cheng, L. et al. Improved estimates of ocean heat content from 1960 to 2015. *Sci. Adv.* **3**, e1601545 (2017).

Publisher's note Springer Nature remains neutral with regard to jurisdictional claims in published maps and institutional affiliations.

Springer Nature or its licensor (e.g. a society or other partner) holds exclusive rights to this article under a publishing agreement with the author(s) or other rightsholder(s); author self-archiving of the accepted manuscript version of this article is solely governed by the terms of such publishing agreement and applicable law.

© The Author(s), under exclusive licence to Springer Nature Limited 2024

Methods

Model and experimental set-up

We isolate the hydrological effect in terms of SSS pattern amplification using two idealized ensemble experiments in the Geophysical Fluid Dynamics Laboratory Earth System Model, version 2M (ESM2M)[54,68,69]. This version uses the Modular Ocean Model 5 with nominal 1° resolution (telescoping to 1/3° at the Equator), Atmospheric Model 2 with 2 × 2.5° resolution, Land Model 3 and the Tracers of Ocean Phytoplankton with Allometric Zooplankton biogeochemical module (full description in the supplemental material of ref. 68). The model is initialized with a multicentury run from the same model, then spun up for approximately 200 model years (the ensemble members begin from consecutive years) with constant pre-industrial atmospheric CO_2 of 286 ppm. Drifts in both physical and biogeochemical variables, estimated from the pre-industrial control run, are within the targets outlined in ref. 68. Specifically, global mean sea surface temperature and SSS have no apparent drift (variability is within ±0.2 K and ±0.02 psu), the global mean ocean temperature drifts by about 0.01 °C per century and globally integrated oxygen content drifts by less than 1% per century. Linear drifts derived from the control run are removed from our results at each grid point.

Two transient ensemble climate change experiments are initialized from the spin-up: Standard and fixed sea surface salinity (Fix-SSS). In the Standard experiment, the atmospheric CO_2 concentration is increased at 1% per year until the CO_2 concentration doubles at year 70, after which the concentration is held fixed for 130 years, so the model run is 200 years long. The Fix-SSS experiment is similar to the Standard run, but SSS is nudged towards the pre-industrial climatology with a freshwater restoring flux (linear in time, with a 30 d timescale). Since the focus here is on changes in precipitation–evaporation tied to the hydrological cycle amplification, SSS is not restored at locations with seasonal sea ice (Extended Data Fig. 9). Freshwater from sea-ice melt that has been transported and led to freshening outside of the region of seasonal sea ice would be restored and attributed to the hydrological cycle amplification in our set-up. This could slightly exaggerate the freshening and consequent impacts in the high-latitude North Atlantic. However, our results suggest that the freshening in this region is due to a decrease in evaporation (Extended Data Fig. 5) associated with the cooling due to AMOC slowdown and that freshwater flux trends due to ice melt are relatively small. This approach, restoring salinity, means that our hydrological effect includes changes in both air–sea fluxes and circulation changes in the atmosphere and ocean. This definition of the hydrological effect can thus be thought of as the total influence of hydrological cycle amplification on the ocean.

The Standard experiment is used to quantify the total effect of climate change on ocean oxygen, which includes the effect of warming, the amplification of the hydrological cycle and other forced changes in the Earth system (for example, sea-ice melt, winds and circulation changes). Note that the freshening at polar latitudes is probably underestimated relative to nature since ESM2M does not incorporate an interactive ice-sheet model. The effect of hydrological cycle amplification is quantified by the difference between the Standard and Fix-SSS experiments. The total climate effect and hydrological effect are designated as ΔX_{Clim} and $\Delta X_{\mathrm{Hydro}}$ for any variable X. For example, $\Delta S_{\mathrm{Hydro}}$ is positive where the ocean gets saltier as the climate system warms and negative where the ocean gets fresher. To reduce the impact of internal variability in the model solutions and extract only the forced response, we run five ensemble members for each experiment branched from different years in the pre-industrial control spin-up experiment (branched from spin-up years 190, 191, 192, 194 and 196). The range across these five ensemble members (Fig. 4) provides an estimate of the influence of internal variability on our results. We also test statistical significance of the trends and find that trends are significantly non-zero at a P value of 0.01 everywhere except narrow transition regions between positive and negative trends (Wald test; python scipy stats.linregress package). Results are shown for the Atlantic Ocean defined by the dark blue mask shown in Extended Data Fig. 9. Model trends are computed over 200 model years (including the 70 years of CO_2 increase and another 130 years of constant CO_2 at 586 ppm) in each member (after removing drift) and then averaged over the five members.

Atlantic water-mass definition

We define Atlantic water masses with density and salinity thresholds on the basis of ref. 51 but slightly adjusted for mean model bias (Extended Data Fig. 8, 9). Tropical waters are defined as all waters lighter than ρ_θ (potential density referenced to the surface) = 1,025 kg m^{-3}. Mode waters are further delimited as lighter than 1,027.6 kg m^{-3}, saltier than 35 psu in the south and saltier than 35.5 psu in the north. Mode waters here include northern and southern subtropical mode waters, as well as the better part of subpolar mode waters in the North Atlantic. Intermediate waters (Antarctic Intermediate Waters) are also lighter than 1,027.6 kg m^{-3} but are generally fresher than 35 psu. In the tropics and below 600 m depth, intermediate waters are limited to be fresher than 34.9 psu, and the volume between intermediate (34.9 psu) and mode (35 psu) waters is defined as deep waters, which upwell near the Equator. Deep waters are defined as all waters denser than 1,027.6 kg m^{-3} but lighter than ρ_2 (potential density referenced to 2,000 dbar) = 1,036.82 kg m^{-3}. This definition of deep waters also includes a fraction of the volume of subpolar mode waters in the North Atlantic. For simplicity, we term these water masses tropical waters, mode waters, intermediate waters and deep waters. The water-mass definitions are stationary in time, determined by the time–mean physical sea state in the 200 yr pre-industrial control run, and capture the distribution of relatively salty (tropical and mode) and relatively fresh (intermediate and deep) water masses in the mean pre-industrial state. The change in salinity largely follows the same contours, although changes in circulation can lead to exceptions, especially in intermediate waters (see Oxygen patterns consistent with ocean circulation changes).

In the observation-based data products, the relevant thresholds in salinity and density are not the same as in the model (which is, for example, biased slightly fresh relative to observations throughout the Atlantic Ocean) but are more similar to the observation-based definitions given by ref. 51 (Fig. 1d,e). Tropical waters are, again, all waters lighter than 1,025 kg m^{-3}. Mode waters in the reanalysis, however, are defined to be saltier than 36.1 psu, warmer than 8 °C and lighter than 1,027.7 kg m^{-3} and intermediate waters are fresher than 34.25 psu and lighter than 1,027.7 kg m^{-3}. Deep waters include the remaining volume between and denser than mode and intermediate waters but lighter than ρ_2 = 1,037 kg m^{-3}. Water denser than this is considered bottom water.

The calculation of potential density (Fig. 5) and attribution of density changes to temperature and salinity (Extended Data Fig. 4) are estimated using the Gibbs Seawater Oceanographic Toolbox[70]: $\rho = \rho(S, \theta)$. Density is calculated from potential temperature and salinity in the corresponding dataset: either ESM2M or the reanalysis. The difference in density due to temperature difference between the Standard and Fix-SSS experiments (Extended Data Fig. 4b) is estimated as the trend in density in the Standard experiment ($\rho_{\mathrm{Std}} = \rho(S_{\mathrm{Std}}, \theta_{\mathrm{Std}})$) minus the trend in density estimated from Standard salinity but Fix-SSS temperature ($\rho_{\mathrm{Std}-\theta} = \rho(S_{\mathrm{Std}}, \theta_{\mathrm{Fix-SSS}})$). The difference in density due to salinity difference between the Standard and Fix-SSS experiments (Extended Data Fig. 4c) is estimated as the trend in density in the Standard experiment ($\rho_{\mathrm{Std}} = \rho(S_{\mathrm{Std}}, \theta_{\mathrm{Std}})$) minus the trend in density estimated from Standard temperature but Fix-SSS salinity ($\rho_{\mathrm{Std}-S} = \rho(S_{\mathrm{Fix-SSS}}, \theta_{\mathrm{Std}})$).

Drivers of O_2 changes

We attribute the changes in oxygen to changes in the saturated oxygen concentration ($O_{2,\mathrm{sat}}$), which is reflective primarily of warming, changes in biological consumption or production of oxygen ($O_{2,\mathrm{bio}}$) and changes in ventilation ($O_{2,\mathrm{vent}}$).

$$\Delta O_2 = \Delta O_{2,\mathrm{sat}} + \Delta O_{2,\mathrm{bio}} + \Delta O_{2,\mathrm{vent}}$$

The $O_{2,sat}$ is estimated from monthly mean conservative temperature and salinity using the Python implementation of the Gibbs Seawater Oceanographic Toolbox for the Thermodynamic Equation of Seawater 10 (TEOS-10) (ref. 70). This calculation assumes saturation at the surface, which is a good assumption for the open ocean, although surface waters may be up to 30% below saturation in coastal waters and highly productive upwelling regions (Fig. 5d,e of ref. 71). The $O_{2,bio}$ is provided by the biogeochemical module of ESM2M (TOPAZ), and $O_{2,vent}$ is derived as the residual. This is very similar to the 'apparent oxygen utilization' methodology (for example, refs. 18,72,73), which groups the effects of biology and circulation together for applications where the impact of biology is unknown.

Data availability

The GFDL ESM2M data used in this study, after pre-processing, are hosted by Dataspace: https://doi.org/10.34770/jw96-r404. The ECMWF Ocean Re-Analysis 5 (ORAS5) data were accessed from the Copernicus Climate Data Store on 5 April 2022 (ref. 58). World Ocean Atlas 2018 (WOA18) oxygen data were accessed from the WOA18 webpage hosted by the NOAA National Centers for Environmental Information on 30 July 2019 (ref. 74).

Code availability

Code for producing figures is available with the data on Dataspace at https://doi.org/10.34770/jw96-r404.

References

68. Dunne, J. P. et al. GFDL's ESM2 global coupled climate–carbon Earth system models. Part II: carbon system formulation and baseline simulation characteristics. *J. Clim.* **26**, 2247–2267 (2013).
69. Griffies, S. et al. ESM2M. GitHub https://github.com/mom-ocean/MOM5 (2020).
70. *The International Thermodynamic Equation of Seawater—2010: Calculation and Use of Thermodynamic Properties* (Intergovernmental Oceanographic Commission, 2010).
71. Duteil, O. et al. A novel estimate of ocean oxygen utilisation points to a reduced rate of respiration in the ocean interior. *Biogeosciences* **10**, 7723–7738 (2013).
72. Boyer, T., Conkright, M. & Levitus, S. Seasonal variability of dissolved oxygen, percent oxygen saturation, and apparent oxygen utilization in the Atlantic and Pacific oceans. *Deep Sea Res. I* **46**, 1593–1613 (1999).
73. Kester, D. R. & Pytkowicz, R. M. Oxygen saturation in the surface waters of the northeast Pacific Ocean. *J. Geophys. Res.* **73**, 5421–5424 (1968).
74. Garcia, H. et al. World Ocean Atlas 2018, Volume 3: Dissolved Oxygen, Apparent Oxygen Utilization, and Dissolved Oxygen Saturation. NOAA National Centers for Environmental Information/National Ocean Data Center Climate Data Online https://data.nodc.noaa.gov/woa (2019).

Acknowledgements

This study was supported by the National Science Foundation Career award 2042672. A.H. acknowledges support from the National Science Foundation Graduate Research Fellowship Program under grant no. DGE-2039656. Any opinions, findings and conclusions or recommendations expressed in this material are those of the author and do not necessarily reflect the views of the National Science Foundation. A.H. also acknowledges support from the Mary and Randall Hack Award at the Princeton University High Meadows Environmental Institute. G.V. and M.L. were supported by award 80NSSC20K0879 from the National Aeronautics and Space Administration. We thank S. Fueglistaler for insightful conversations, which greatly improved the manuscript and inspired the addition of Fig. 4.

Author contributions

A.H., L.R., G.V. and M.L. conceived of the work and experiments; A.H. and L.R. led the analysis and writing.

Competing interests

The authors declare no competing interests.

Additional information

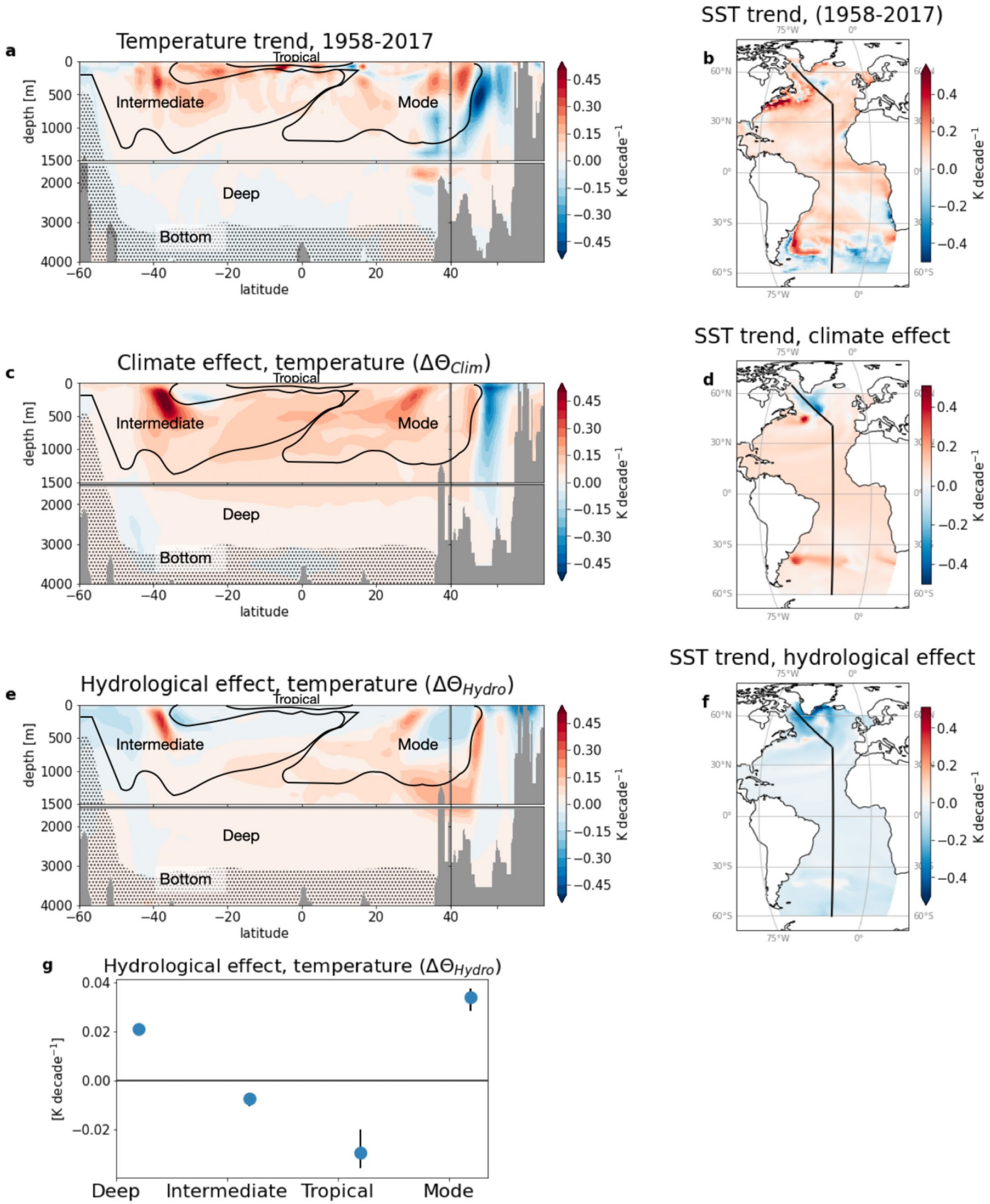
Extended data is available for this paper at https://doi.org/10.1038/s41558-023-01897-w.

Correspondence and requests for materials should be addressed to Allison Hogikyan.

Peer review information *Nature Climate Change* thanks Lijing Cheng, Esther Portela and Nikolaos Skliris for their contribution to the peer review of this work.

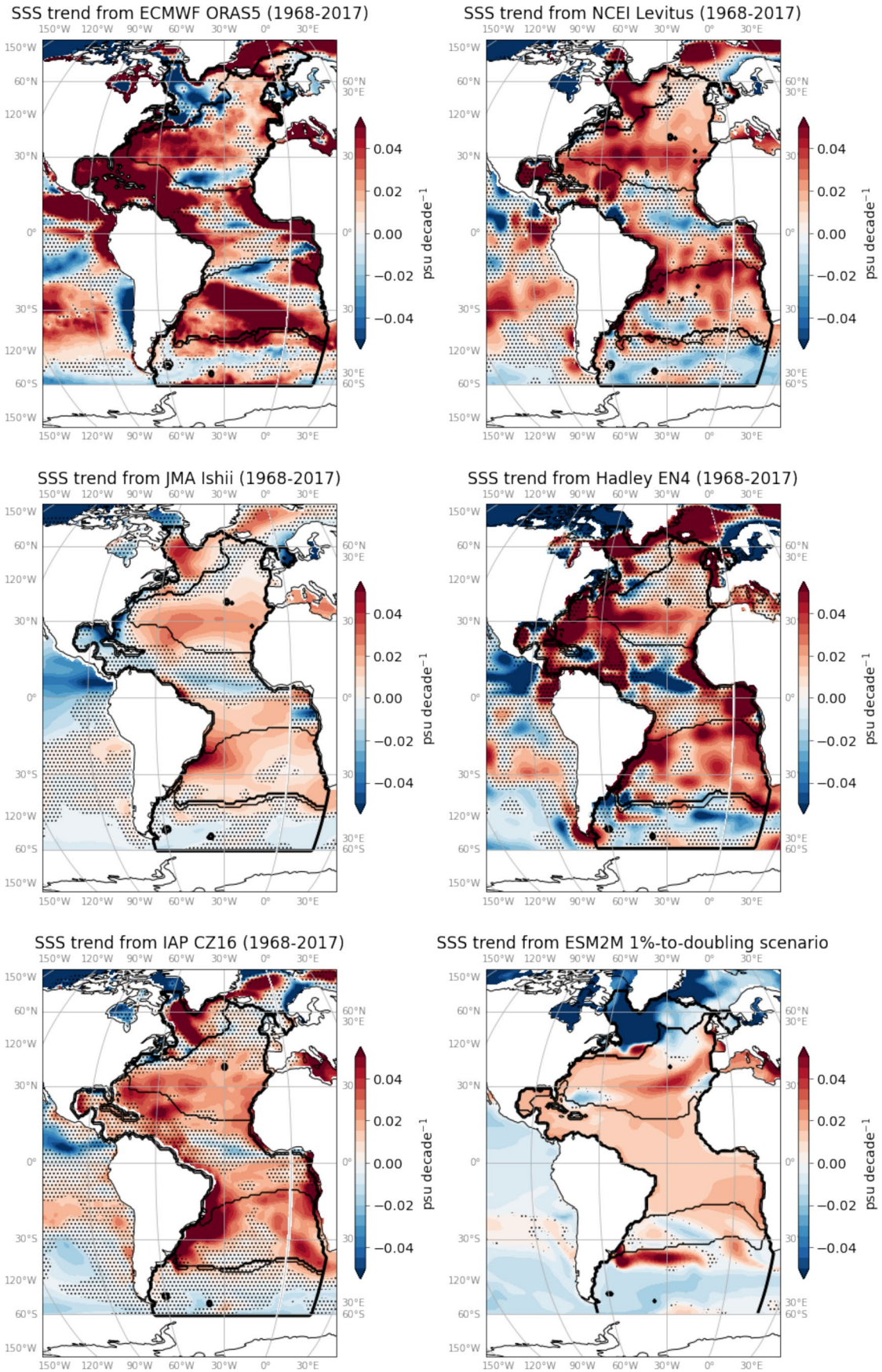
Reprints and permissions information is available at www.nature.com/reprints.

https://doi.org/10.1038/s41558-023-01897-w



Extended Data Fig. 1 | Warming along mid-Atlantic Ocean section. (a) ESM2M temperature trend due to total climate effect (200-year trend in the Standard experiment, averaged across 5 members), (b) ESM2M temperature trend due to hydrological effect (Difference in 200-year trends between the Standard and Fix- SSS experiments, averaged over 5 members for each experiment), (c) ORAS5 historical temperature trend (1958-2017). SST trend in (d) climate effect, (e) hydrological effect, (f) ORAS5 historical period.

https://doi.org/10.1038/s41558-023-01897-w

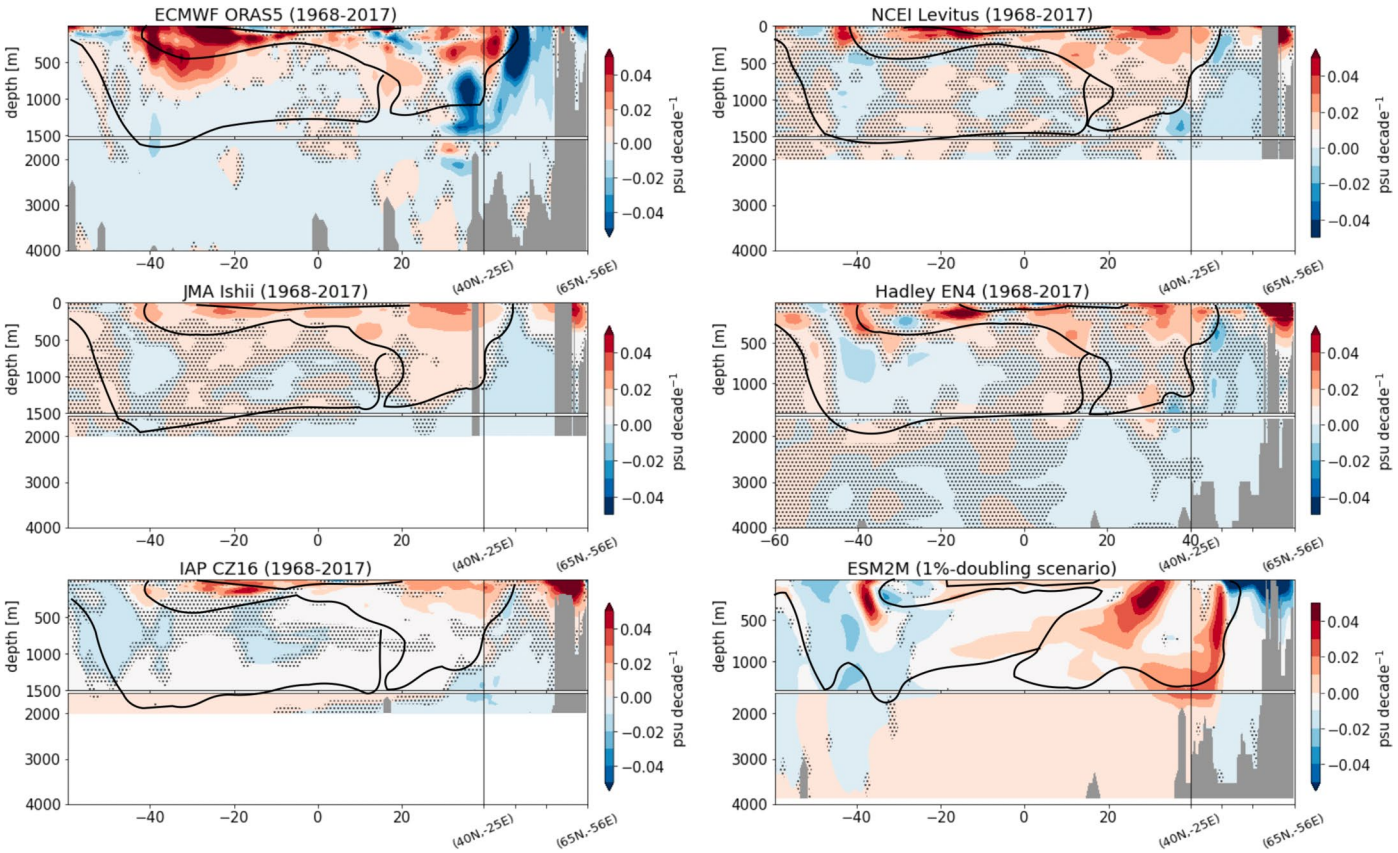


Extended Data Fig. 2 | See next page for caption.

https://doi.org/10.1038/s41558-023-01897-w

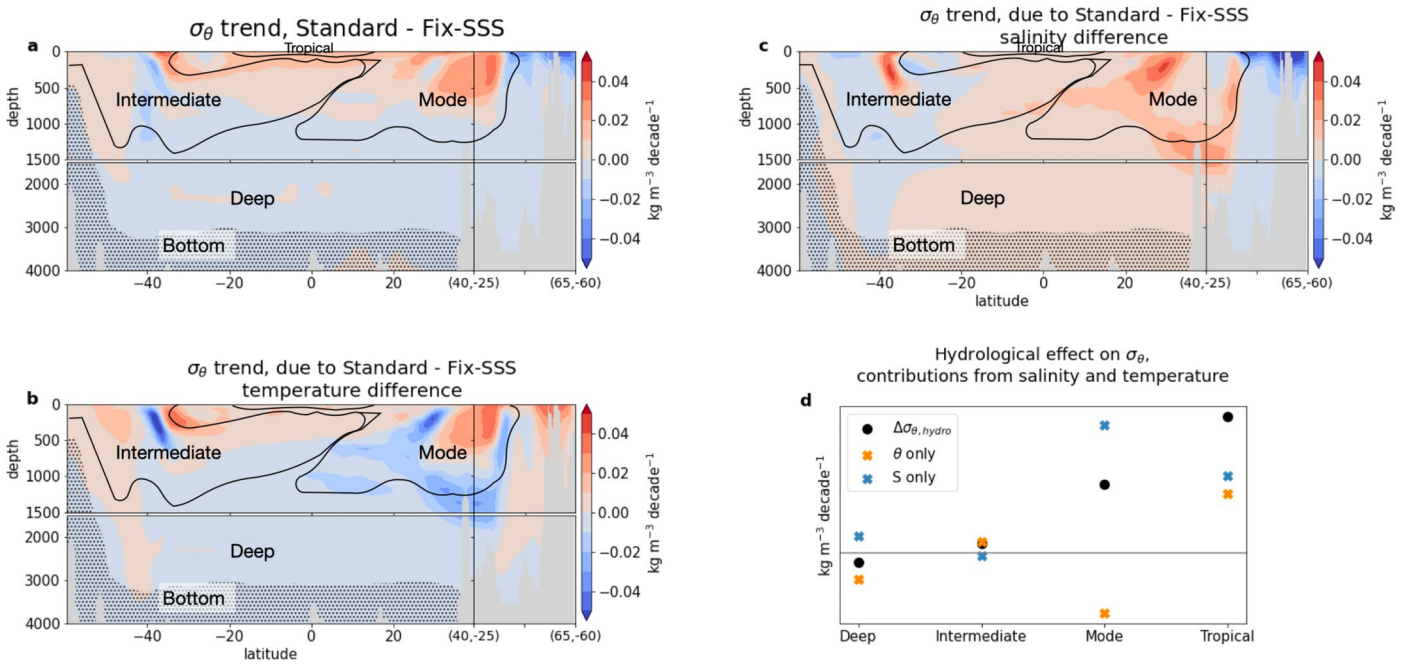
Extended Data Fig. 2 | Sea surface salinity trend in observation-based datasets and climate model. Stippling in each panel indicates that the trend is not significant at the 95% confidence level. Datasets are as follows: ECMWF's reanalysis ORAS5[4], National Center for Environmental Information's objective analysis Levitus[5], Japanese Meteorological Agency's objective analysis Ishii[6], UK-Hadley Centre's objective analysis EN4[7], and Institute for Atmospheric Physics' objective analysis CZ16[8]. The final, lowest right, panel shows the 200-year trend in the ESM2M 1%-to-doubling experiment used in this study. Black contours show water masses according to density and salinity criteria outlined in Methods section, using the mean density and salinity in each dataset (for Levitus, the World Ocean Atlas 2018 dataset is used). Area south of 60∘S has been removed.

https://doi.org/10.1038/s41558-023-01897-w



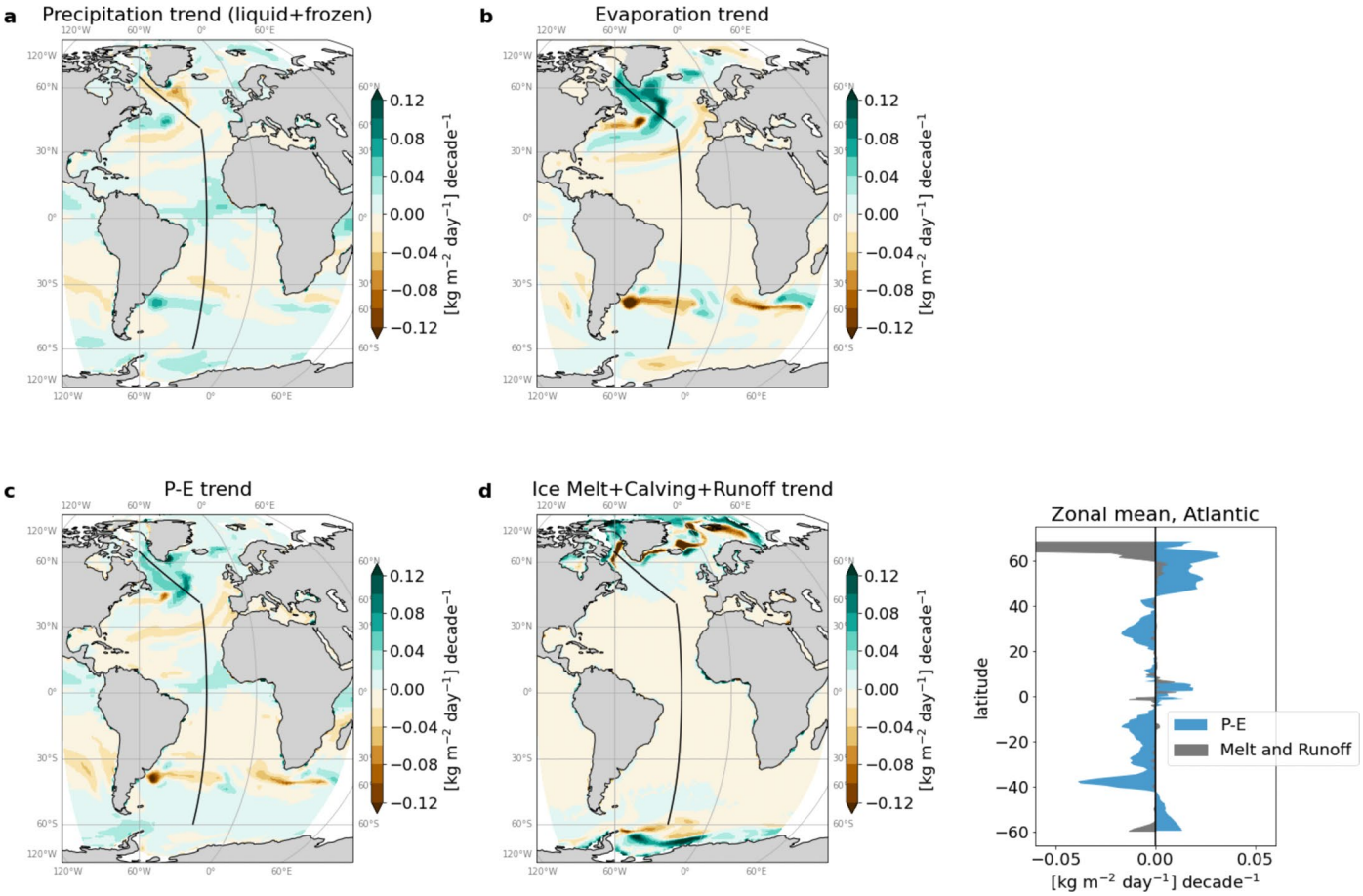
Extended Data Fig. 3 | Salinity trend in observation-based datasets and climate model, following the trajectory along 25°W shown in Figure 1. Stippling in each panel indicates that the trend is not significant at the 95% confidence level. Datasets are as follows: ECMWF's reanalysis ORAS5[4], National Center for Environmental Information's objective analysis Levitus[5], Japanese Meteorological Agency's objective analysis Ishii[6], UK-Hadley Centre's objective analysis EN4[7], and Institute for Atmospheric Physics' objective analysis CZ16[8]. The final, lowest right, panel shows the 200-year trend in the ESM2M 1%-to-doubling experiment used in this study. Grey areas are bathymetry and white areas are missing data. Black contours show water masses according to density and salinity criteria outlined in Methods section, using the mean density and salinity in each dataset (for Levitus, the World Ocean Atlas 2018 dataset is used).

https://doi.org/10.1038/s41558-023-01897-w



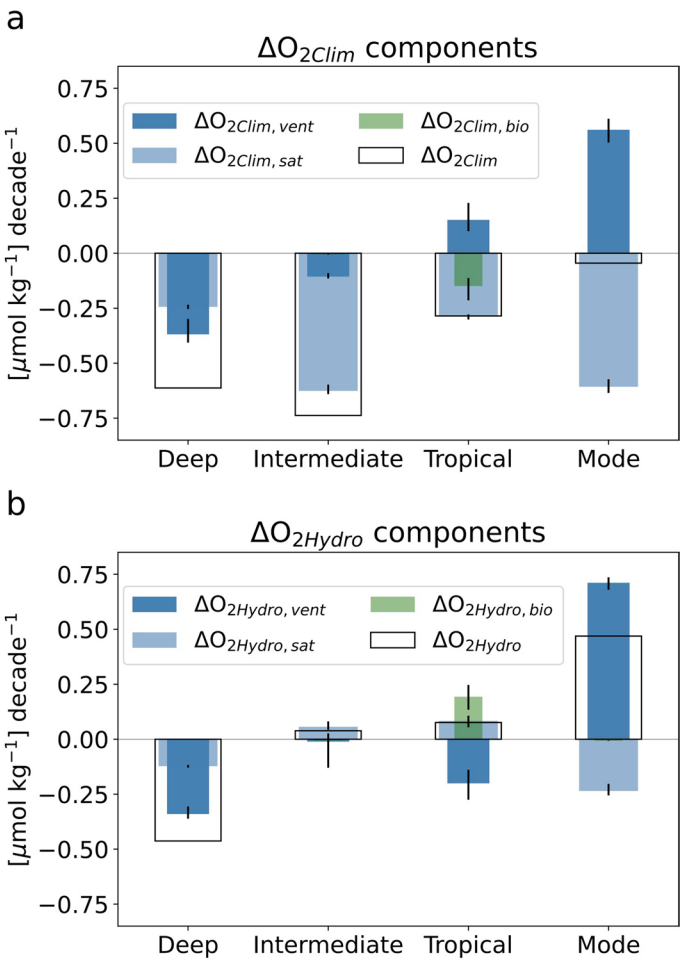
Extended Data Fig. 4 | Hydrological effect on potential density, and contributions from temperature and salinity changes. (a) Hydrological effect (200-year linear trends in Standard - Fix-SSS) on potential density referenced to the surface σ_θ, along 25∘W, as in Figure 4. (b) Potential density trend associated with the hydrological effect but due to (b) changes in temperature alone (temperature from Standard trajectory but salinity from Fix-SSS) and (c) changes in salinity alone (salinity from Standard trajectory but temperature from Fix-SSS). (d) Average difference in potential density, and contributions from salinity and temperature in each water mass. Densities computed with the gsw toolbox[9]. The section in panels a-c follows the black line shown on maps in Extended Dataset Figure 1. All for five-member ensemble mean.

https://doi.org/10.1038/s41558-023-01897-w



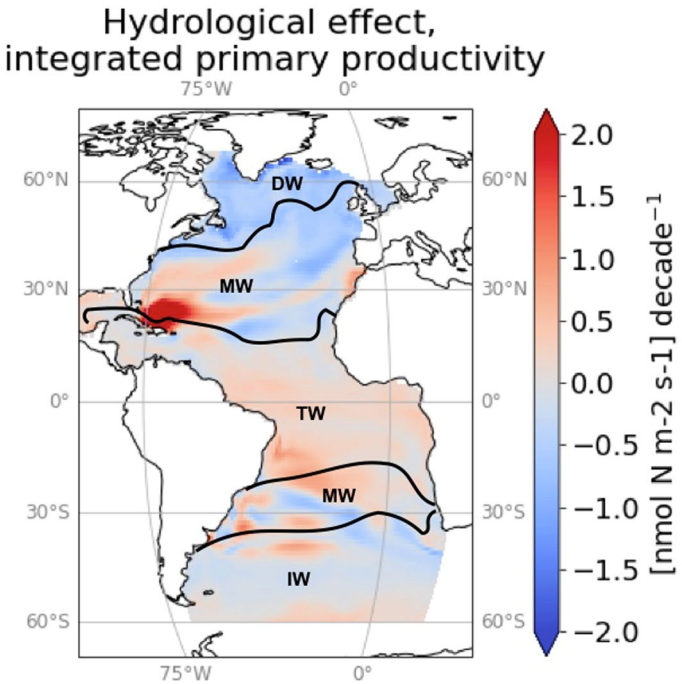
Extended Data Fig. 5 | Freshwater flux trends in response to CO_2 forcing. 200-year freshwater flux trends in the ensemble-mean Standard 1%-to-doubling experiment. (a) Precipitation, (b) evaporation, (c) the net of precipitation - evaporation, and (d) the remaining fluxes from ice melt, ice calving, and runoff. (e) Zonal mean trend due to precipitation - evaporation (blue), which broadly follows the dry-get-drier, wet-get-wetter pattern, and the zonal mean of other components (grey).

https://doi.org/10.1038/s41558-023-01897-w



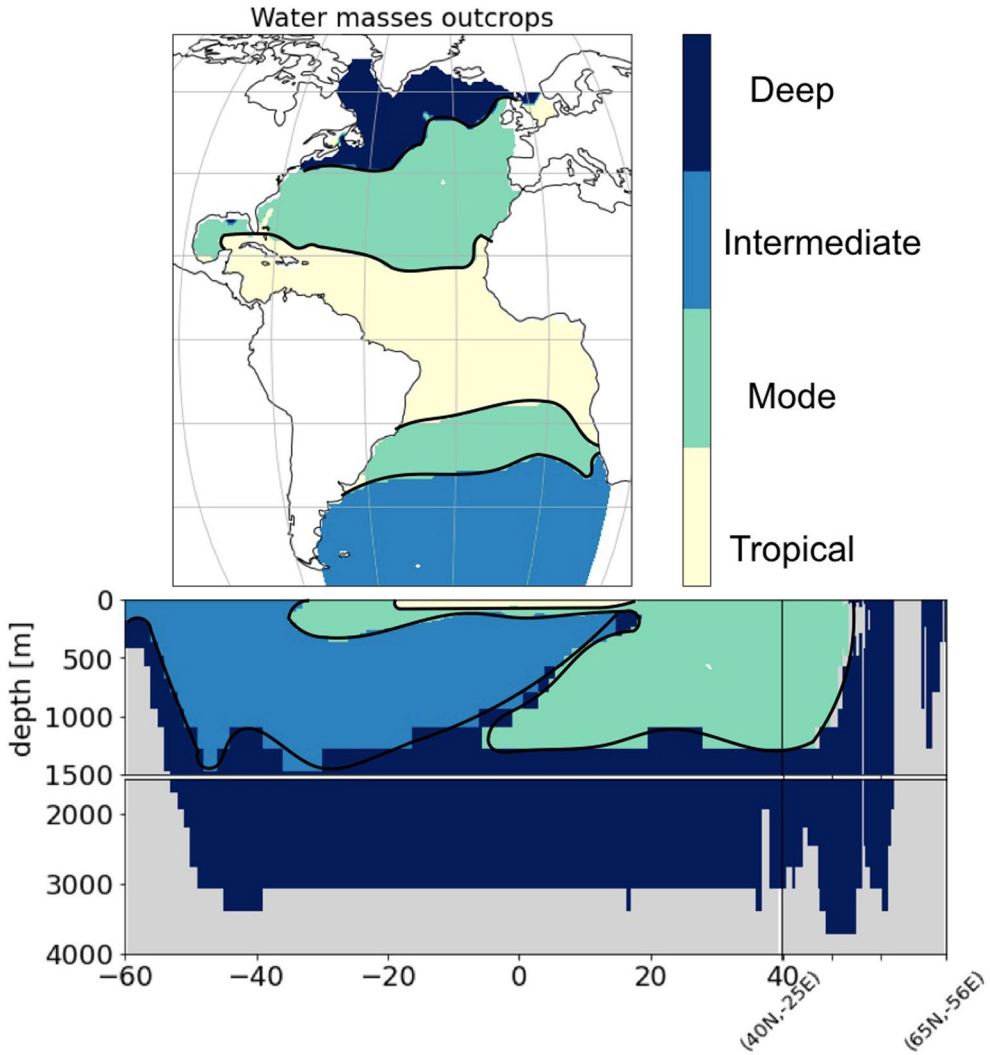
Extended Data Fig. 6 | Mean trends in (de)oxygenation and drivers. (a) Model contributions to climate effect on oxygen changes (ΔO_{2Hydro} in black contours) attributed to changes in ventilation ($\Delta O_{2Hydro,vent}$, dark blue), solubility ($\Delta O_{2Hydro,sat}$, light blue) and biological activity ($\Delta O_{2Hydro,bio}$, green). $\Delta O_{2Hydro,bio}$ is only visible in Tropical Waters because it is 2-4 orders of magnitude smaller than the other terms in other water masses. (b) Ensemble mean change in oxygen in Atlantic Ocean water masses due to hydrological effect, reproduced from Figure 3c. Error bars represent the range across five ensemble members.

https://doi.org/10.1038/s41558-023-01897-w



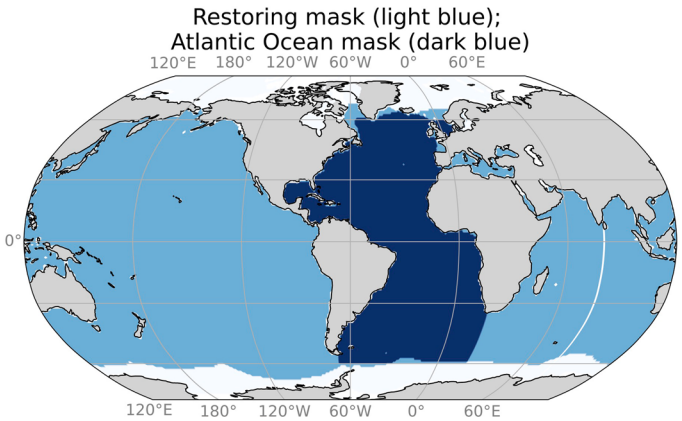
Extended Data Fig. 7 | Trend difference in primary productivity. Vertically integrated 200-year trend in primary productivity, Standard 1% minus Fix-SSS experiment. Note that primary productivity is limited to the sunlit region of the ocean, thus the vertical integral represents production in near-surface waters.

https://doi.org/10.1038/s41558-023-01897-w



Extended Data Fig. 8 | Mask of water masses in Atlantic Ocean. Defined with 100-year annual average fields in the ESM2M pre-industrial control experiment, as described in Methods. Black contours are the smoothed water mass limits visualized in all other figures.

https://doi.org/10.1038/s41558-023-01897-w



Extended Data Fig. 9 | Mask of SSS restoring location, and Atlantic Ocean. Global restoring of sea surface salinity is only applied in the light and dark blue locations, but is not applied where there is seasonal sea ice in pre-industrial control run (white regions). Dark blue mask based on 'regionmask' Python package is used to isolate Atlantic Ocean water masses in Figures 2, 4, and Extended Data Figure 3.